

Article

Effective Promotion of Micro Damping of GO Hybrid PU–PF Copolymer Grinding Wheels on Precision Machining

Shaoling Xia ^{1,*}, Hongying Zhang ¹, Jixian Xu ², Yingliang Liu ³, Cong Liu ¹, Shengdong Guo ¹, Xudong Song ^{1,*}, Jin Peng ¹, Yu Jia ¹ and Jialu Li ¹

¹ School of Materials Science and Engineering, Henan University of Technology, Zhengzhou 450001, China; m13253392659_1@163.com (H.Z.); 15294763611@163.com (C.L.); 17549213027@163.com (S.G.); jin_peng@haut.edu.cn (J.P.); jiyu@stu.haut.edu.cn (Y.J.); 221071000230@stu.haut.edu.cn (J.L.)

² Langfang Shengsen Grinding Tools Co., Ltd., Langfang 065900, China; 13513012175@163.com

³ School of Materials Science and Engineering, Zhengzhou University, Zhengzhou 450052, China; liuylxn@zzu.edu.cn

* Correspondence: shaoling_xia@haut.edu.cn (S.X.); xudong_song@haut.edu.cn (X.S.); Tel./Fax: +86-371-6775-8721 (S.X.)

Abstract: The influence of damping and friction performance of grinding wheels on precision grinding was explored for the first time. GO hybrid PU-modified PF copolymers were prepared by in situ synthesis and adopted as a matrix for fabricating grinding wheels. FT-IR, DSC, TG, and mechanical property tests showed the optimal modification when PU content was 10 wt% and GO addition was 0.1 wt%. Damping properties were investigated by DMA, and tribological characteristics were measured by sliding friction and wear experiments. The worn surfaces and fracture morphologies of GO hybrid PU–PF copolymers were observed by SEM. Distribution of components on the worn surfaces was explored by Raman mapping and EDS. The research results revealed that the PU component tended to be dispersed around the edges of corundum abrasives acting as a buffer layer of abrasive particles, which could provide micro-damping characteristics for abrasives, making the grinding force more stable during precision machining and facilitating a smoother surface quality of the workpiece.

Keywords: damping; tribological characteristics; graphene oxide; precision machining



Citation: Xia, S.; Zhang, H.; Xu, J.; Liu, Y.; Liu, C.; Guo, S.; Song, X.; Peng, J.; Jia, Y.; Li, J. Effective Promotion of Micro Damping of GO Hybrid PU–PF Copolymer Grinding Wheels on Precision Machining. *Coatings* **2024**, *14*, 632. <https://doi.org/10.3390/coatings14050632>

Academic Editor: Alexander Tolstoguzov

Received: 17 April 2024

Revised: 13 May 2024

Accepted: 13 May 2024

Published: 16 May 2024



Copyright: © 2024 by the authors. Licensee MDPI, Basel, Switzerland. This article is an open access article distributed under the terms and conditions of the Creative Commons Attribution (CC BY) license (<https://creativecommons.org/licenses/by/4.0/>).

1. Introduction

Precision machining is an important link in the development of contemporary science [1] that plays a crucial role in contemporary high-tech fields and military and civilian industries, especially in the field of electrical automation, such as ultra-large-scale integrated circuits, high-precision disks, precision radars, missile fire control systems, precision instruments, optical lens, copier drums, etc. [2–7]. Its development trend has been from micrometer and submicron scales towards nanoscale processing technology [8–10]. In order to achieve satisfactory machining accuracy, machine tools, especially grinding wheels, need to have excellent dynamic performance and chatter avoided as much as possible [11,12]. Chatter in machining processes is strongly dependent on the dynamic compliance behavior of the machine tool and workpiece. The critical cutting depth where chatter occurs is in inverse proportion to the absolute value of the negative real part of the complex dynamic compliance response function of the machine tool. Therefore, while designing a machine tool, active damping systems should be designed to help avoid chatter of the machine tool [13]. Numerical structural models were established to analyze the contribution of vibration damping to machine tools [14]. Some scholars increased damping property by mounting the abrasive rim of the wheel via a flexible coupling or by modifying the flexibility of the grinding wheel shaft device [15–17]. These attempts have been successful, and the grinding accuracy and surface quality of the workpiece have been further improved. Since

good damping characteristics have been proven to be beneficial for improving machining results [18–23], in theory, improving the damping performance of the grinding wheel itself could further improve the precision machining effect.

With excellent damping property, polyurethane (PU) has attracted much interest from researchers for use in damping and vibration isolation [24–28]. It was widely explored as a modifier to improve the damping performance of other polymer materials, such as epoxy [29–34], polystyrene [35], poly(tetramethylene glycol) [36], vinyl ester resin/ethyl acrylate [37], poly(vinylidene fluoride) [38], and so on. These studies achieved satisfactory results, but there have been few reports on enhancing damping properties of phenol formaldehyde resin (PF) by PU modification. As is well known, due to its excellent strength, rigidity, heat resistance, wear resistance, and low cost, PF is widely used as a matrix material for grinding tools. The drawback of PF grinding tools is the lack of damping, which is not conducive to obtaining fine surface quality of a workpiece in precision grinding. We attempted to improve the machining effect of the grinding wheel by increasing the damping property of PF through PU modification.

On the other hand, the formation of a self-lubricating layer by adding lubricants can reduce friction between the grinding wheel and workpiece, improving the surface quality of a workpiece [39]. As far as lubricants are concerned, graphene oxide (GO) cannot be ignored. The superior mechanical properties and high thermal conductivity of GO led to its excellent tribology applications in polymer nanocomposites [40,41]. The atomically smooth surface and weak van der Waals force between the GO layers eased interlayer sliding and contributed to its self-lubrication characteristics [42,43]. Furthermore, our previous work displayed that a 2D structure of GO with high specific surface area was also good for load transferring [44,45].

In this paper, in order to enhance damping and vibration properties, PU-modified PF copolymers were synthesized as the matrix of grinding wheels. GO was also introduced into the system to improve the tribology and grinding performance of materials. We conducted comprehensive characterization and tests of the GO hybrid PU–PF copolymers and conducted precision grinding experiments, which showed excellent machining results. This paper focuses on exploring the copolymers' damping characteristics, friction performance, and their impact mechanism on precision machining.

2. Experimental

2.1. Materials

Pre-polyurethane (PPU) with NCO content of 4% was supplied by Henan Institute of Chemistry. Phenol was obtained from Chengdu Kelong Chemical Co., Ltd. (Chengdu, China), formaldehyde (37%) and polyformaldehyde were supplied by Xilong Science Co., Ltd. (Chengdu, China), and hydrochloric acid (HCl) was purchased from Henan X.Z.C Reagent Ltd. (Zhengzhou, China). Dibutyltin dilaurate was produced by Ningxia Lingshi New Material Technology Co., Ltd. (Ningxia, China). All the materials were of analytical purity and used without purification.

2.2. *In Situ* Synthesis of GO Hybrid PU–PF Copolymers

PU–PF copolymer was firstly synthesized as shown in Figure 1A. PPU, phenol, and dibutyltin dilaurate catalysts were added to a flask and heated to 76 °C for 2 h. Then, the temperature was reduced to 60 °C, formaldehyde was added to the flask (the mole ratio of phenol to formaldehyde was 7:6), and a 25% HCl aqueous solution was added to the mixed solution four times. The interval each addition was 1 h, and the reaction temperatures were 75 °C, 80–85 °C and 95 °C, each temperature lasting for 2 h. After the reaction reached the end point, the product was put into a vacuum-drying oven and dried at 120 °C for 2 h. After cooling, a light-yellow translucent solid was obtained. This procedure has been proved to be effective in our previous research [46]. In that paper, a series of PU–PF copolymers with PU content of 0 wt%, 5 wt%, 10 wt%, 15 wt%, and 20 wt% were synthesized. Among them, 10 wt% content displayed the optimal mechanical properties, such as hardness, bending

strength, and impact strength. As such, in this study, we selected 10 wt% PU content in the PU–PF copolymer as the matrix of GO-hybridized copolymer.

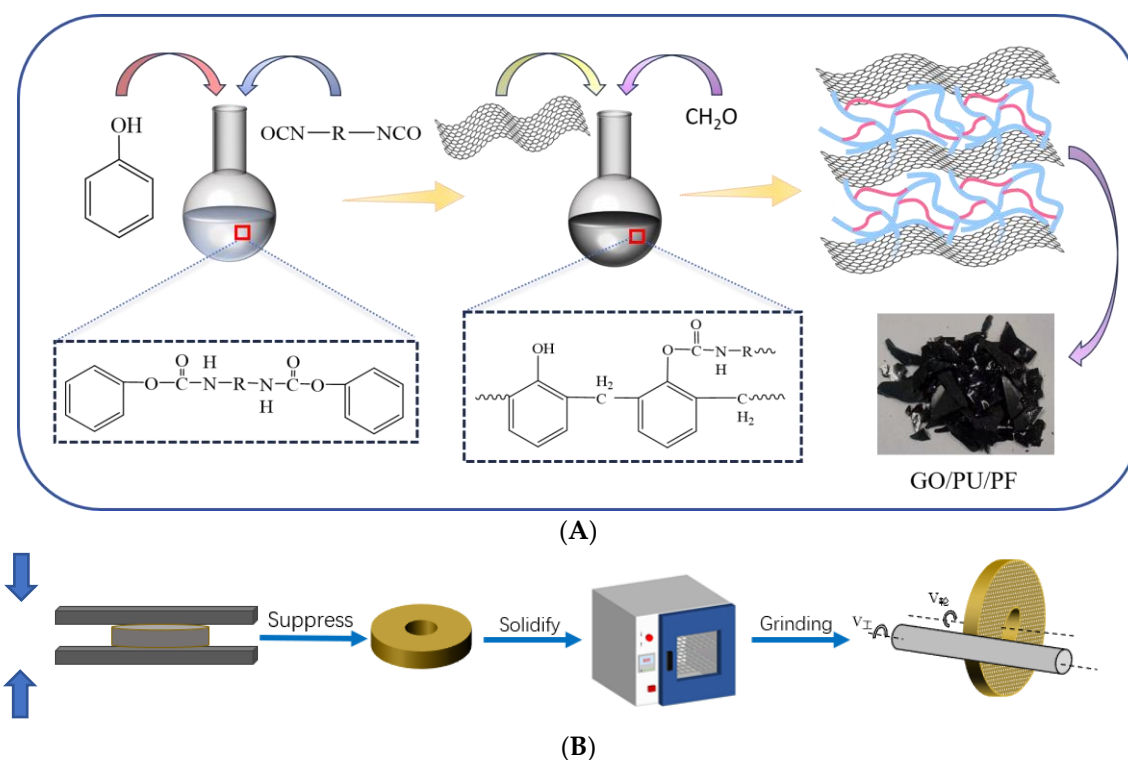


Figure 1. Scheme of synthesis of GO hybrid PU–PF copolymer (A) and fabrication of grinding wheels (B).

As for the preparation of GO hybrid PU–PF copolymers, GO was synthesized from graphite through a modified Hummers method according to our previous procedure [44,45] and kept in deionized water as a suspension form. The GO suspension was directly mixed with formaldehyde, and the other experimental procedures were the same as described above. A series of GO hybrid PU–PF copolymers with different GO content of 0.05 wt%, 0.1 wt%, 0.15 wt%, and 0.2 wt% were synthesized. The resultant GO hybrid PU–PF copolymer was black powder. Polyformaldehyde was added to the resultant powder as curing agent.

Grinding wheels, as well as samples for mechanical and DMA testing, were fabricated as shown in Figure 1B. GO hybrid PU–PF copolymers, corundum abrasive, and hollow ball filler were mixed into the mold at a volume ratio of 4:5:1, heated to 110 °C in flat vulcanizer, flattened and kept at 180 °C for 30 min, then demolded after natural cooling. Then, the samples were secondary cured at 120 °C, 140 °C, 160 °C and 180 °C for 2 h.

2.3. Testing Methods

FT-IR (Shimadzu, IR Prestige-21, Kyoto, Japan) was employed to study the chemical structure of GO hybrid PU–PF copolymer at a resolution of 0.5 cm^{−1}. TG (Peking Optical Instrument Factory, WCT-2, Beijing, China) and DSC (NETZSCH, 200F3, Selb, Germany) were tested with a heating rate of 10 °C/min in air. Dynamic thermomechanical analysis (DMA, NETZSCH, DMA242C, Selb, Germany) was used to investigate the dynamic mechanical properties using the compassing mode at a frequency of 45 Hz and at a heating rate of 3 °C/min. Tensile strength and elongation were tested by a tensile instrument (Jinan Faen Instrument Factory, WDW-S, Ji’nan, China) according to GB/T 528-1998 [47]. The bending strength was tested by 3-point support mode. Tribology characteristics was studied by a pin-on-disk friction wear testing machine (Lanzhou Zhongke Co., Ltd., Lanzhou, China,

QG-700) at room temperature in dry conditions. The counterpart pin is fabricated by steel with a diameter of 5 mm. The normal load and sliding speed were 0.4 MPa and 0.5 m/s, respectively. Experimental data were collected during 60 min of wearing for disk-like samples with a diameter of 60 mm and a thickness of 5 mm. Precision machining experiments were carried out using a CNC cylindrical grinder (MK1320C-500, Wuxi Yulin Machine Tool Co., Ltd., Wuxi, China). The worn surfaces and fracture morphologies of GO hybrid PU–PF copolymers were observed by SEM (Inspect F50, Thermo Fisher Scientific, Waltham, MA, USA). Distribution of components in grinding wheels was revealed by energy-dispersive spectroscopy (EDS). Chemical changes on the worn and unworn surfaces were explored via Raman mapping (Thermo Fisher Scientific DXRxi Raman imaging spectrometer) at a laser wavelength of 633 nm with laser energy of 4.3 MW. The wave-number range of Raman spectra was 0–3000 cm^{-1} with a spectral resolution of 1 cm^{-1} .

3. Results and Discussion

3.1. Fabrication of GO Hybrid PU–PF Copolymers

GO was synthesized by the same method as our previous research, and its characterization results are given in papers published by our research group [44,45]. The GO hybrid PU–PF copolymers prepared in this study were characterized by FI-IR, TG, and DSC. Mechanical properties were also tested. The results are shown in Figure 2.

The FT-IR spectra of pure PF, PPU, GO, and GO hybrid PU–PF copolymer are shown in Figure 2A. In the GO hybrid PU–PF copolymer spectra, strong C–H and –C=O stretching vibration peaks in PU chains appeared at 2943 cm^{-1} , 2860 cm^{-1} and 1708 cm^{-1} , respectively, but the stretching band of the isocyanate group (NCO) at 2274 cm^{-1} disappeared on the spectra of GO hybrid PU–PF copolymer, implying the –NCO groups in PU completely reacted with –OH groups in phenol.

The thermal stability of resulting nanocomposites was investigated by TG. The TG curves of PU–PF (a), GO hybrid PU–PF copolymers with different GO weight content 0.05 wt% (b), 0.1 wt% (c), 0.15 wt% (d), 0.2 wt% (e), and GO (f) are shown in Figure 2B. Data on characteristics are summarized in Table 1. It is obviously in Figure 2B that the curves moved to the right with the increase in GO content, which meant an increase in thermal stability. Both 20% and 50% weight-loss temperature were significantly increased with the increase GO content. The semi-disassembly temperatures of GO hybrid PU–PF copolymers with GO content of 0 wt%, 0.05 wt%, 0.1 wt%, 0.15 wt%, and 0.2 wt% were 528 °C, 543 °C, 565 °C, 580 °C, and 595 °C, respectively. This was attributed to strong intermolecular interactions, such as hydrogen bonds or van der Waals forces, between PF, PU, and GO, also acting as cross-linking points that could limit the movement of chain segments and consequently enhance the thermal stability.

Table 1. Temperatures of 20% and 50% weight loss in PU–PF (GO 0 wt%) and GO hybrid PU–PF copolymers with different GO content.

Weight-Loss Rate	GO wt%				
	0	0.05	0.1	0.15	0.2
20%	405	428	424	486	482
50%	528	543	565	580	595

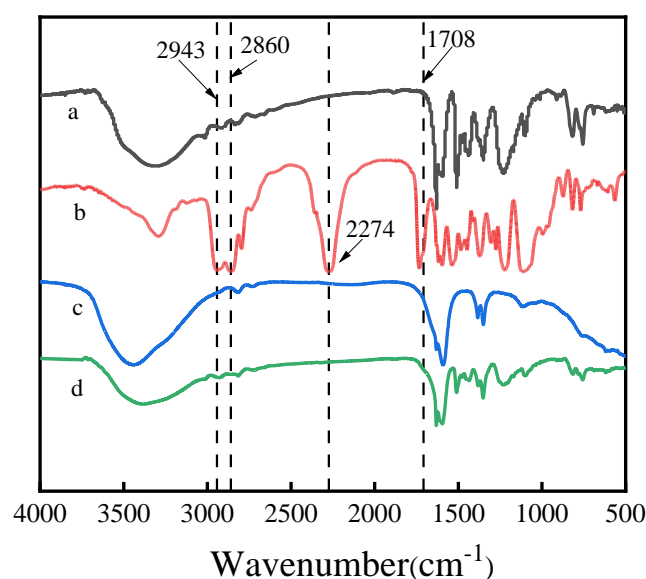
The DSC curves of GO hybrid PU–PF copolymers with different GO content are shown in Figure 2C. Melting peaks can be seen below 100 °C. The peaks that appear between 140 °C and 170 °C were considered to be curing reaction peaks. Table 2 shows the temperature corresponding to the lowest point of the peak in Figure 2C, that is, the curing temperature. As can be seen from Figure 2C and Table 2, when GO content was below 0.1 wt%, the curing temperature increased with the increase in GO content, but they tended in the opposite direction when GO content were more than 0.1 wt%. The curing temperature reached the highest value of 159 °C when the GO content was 0.1 wt%. The reason

was conjectured as following: when GO content were below than 0.1 wt%, GO pieces could be evenly intercalated between the PF and PU molecular chains, which resulted in the enlargement of the space between PF and PU molecular chains, and the distance between the reaction groups became further apart. What's more, the GO intercalation could also inhibit the movement of polymer molecular chains, so that the cross-linking reactions were more difficult to generate, resulting in the increment of curing temperature. When the GO content continued to increase, GO concentration became too high, resulting in agglomeration and accumulation, so that it could not be evenly intercalated between the polymer chains and begin to produce phase separation with the polymers, so the influence on the distance between the reaction groups and the hindrance of the molecular chains was weakened, and the cross-linking reaction was easier to occur, so the curing temperature began to decrease with further increase in GO content.

Table 2. Curing temperatures of PU–PF (GO 0 wt%) and GO hybrid PU–PF copolymers with different GO content.

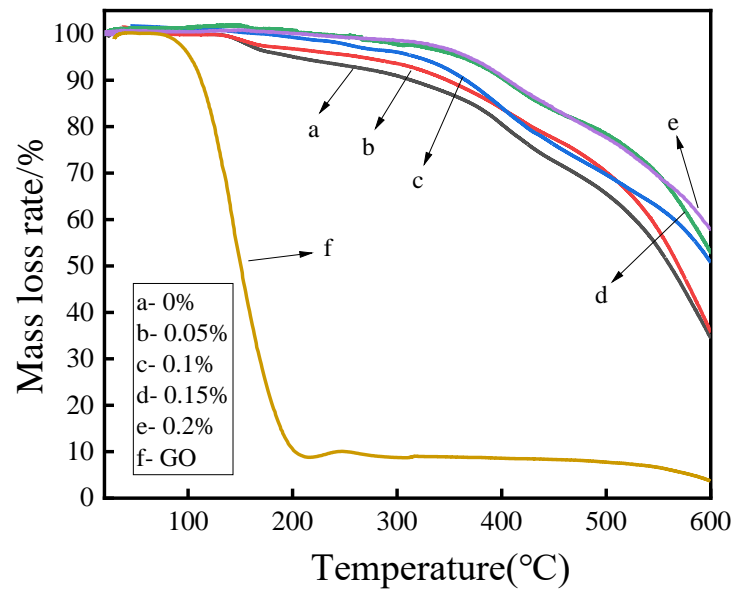
GO Content	0 wt%	0.05 wt%	0.1 wt%	0.15 wt%	0.2 wt%
Curing temperatures	148 °C	150 °C	159 °C	155 °C	154 °C

Mechanical properties test also displayed the same tendency. Figure 2D showed bending strength and impact strength of GO hybrid PU–PF copolymers with different GO content. Both bending strength and impact strength reached the maximum when the GO content was 0.1 wt%. Compared to the PU–PF copolymer without the GO hybrid, bending strength was enhanced by 14.8% and impact strength was enhanced by 18.8%. This phenomenon confirms our previous suspicions. We believe that 0.1 wt% GO content was optimal for the even intercalation of GO pieces in the PU–PF copolymer chains. The unique layer structure of GO and the molecular interaction between GO and copolymer chains effectively transferred the stress, reduced distortion and fracture, and thus improved the mechanical properties, but too much GO hybrid caused agglomeration, resulting in stress concentration, which led to the reduction in mechanical properties.

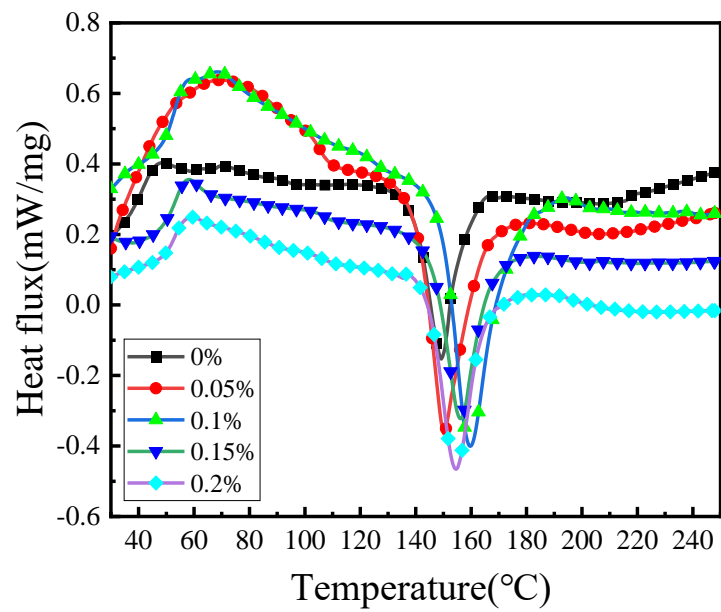


(A)

Figure 2. Cont.



(B)



(C)

Figure 2. Cont.

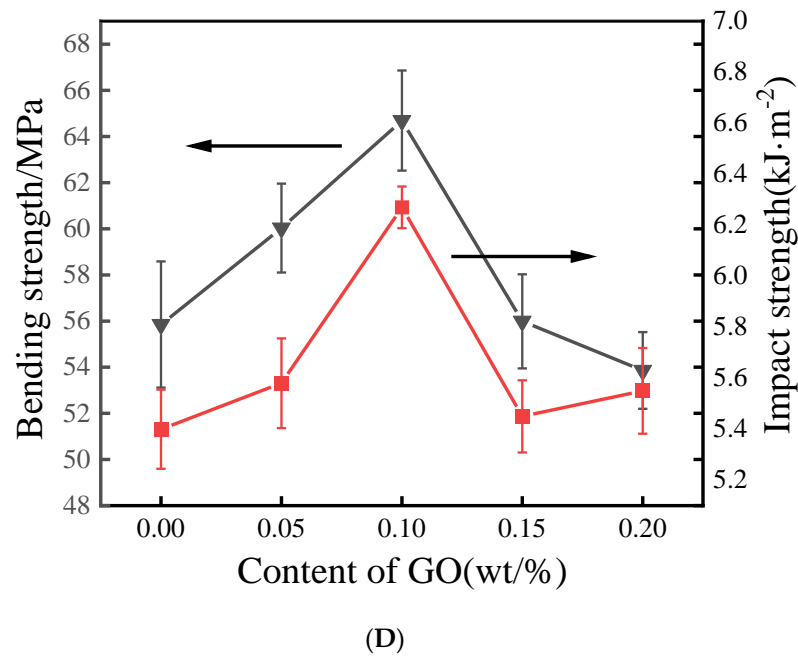


Figure 2. FT-IR spectra (A) of pure PF (a), PPU (b), GO (c) and GO hybrid PU–PF copolymer (d), TG (B), DSC (C) and bending/impact strength (D) of resultant materials.

3.2. Damping Property

DMA was detected at a frequency of 45 Hz, which corresponded to 35 m/s rotational speed of the grinding wheel during precision machining. As shown in Figure 3A, the rectangular shaded area lay in the range of the precision machining temperature. It can be seen in this area that there is a huge peak on the curve of PU (a), which is completely nonexistent on the curve of PF (c). But on the curve of PU–PF copolymer (b) that contained 10 wt% PU, a small peak appears. This peak resulted from the glass transition of PU, which meant some segments on PU were able to move gradually. This result indicates that the PU ingredients endowed the PU–PF copolymer with micro damping properties.

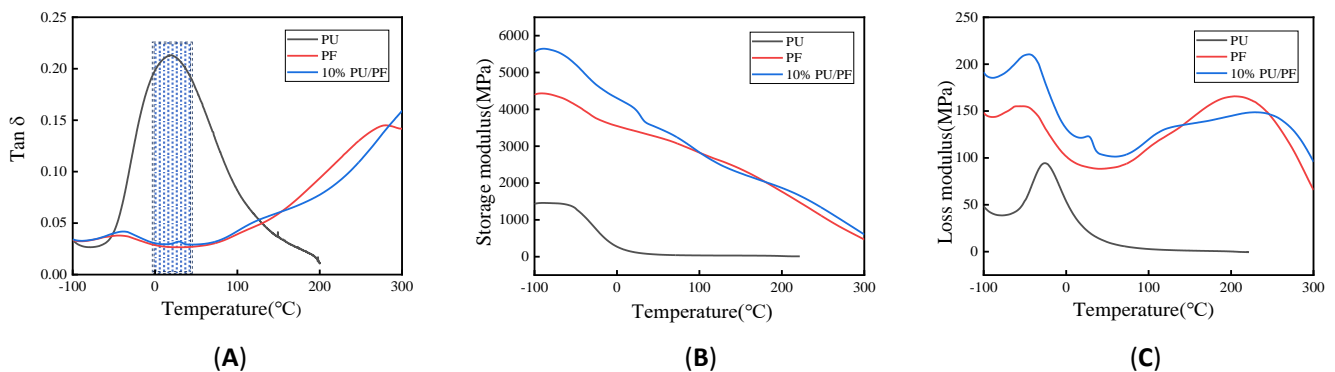


Figure 3. Tan δ (A), energy storage modulus (B), and loss modulus (C)—temperature curves of PU, PF, and PU–PF copolymer.

Figures 3B and 3C respectively, display the energy storage and loss modulus–temperature curves of PU, PF, and PU–PF copolymer. The two graphs show the same phenomenon in that both storage modulus and loss modulus of the copolymer were greater than that of each homopolymer at room temperature. This meant that both elasticity and viscosity of the copolymer had been significantly improved.

For different GO-content samples of GO hybrid PU–PF copolymers, it can be seen in Figure 4A that glass transition peaks almost appear at room temperature, but no glass

transition peak appeared on the curve of 0.2 wt% GO-content PU–PF copolymer. To explore the reason, we checked their energy storage and loss modulus–temperature curves (Figure 4B,C). It was found that an energy storage modulus of the 0.2 wt% GO-content sample was the maximum in all the GO content samples tested, but its loss moduli were lower than that of 0.1 wt% and 0.15 wt% GO-content samples. Since $\text{Tan}\delta$ is a quotient of loss modulus and storage modulus, the $\text{Tan}\delta$ of 0.2 wt% GO content sample was reduced. It was presumed that a large number of GO pieces intercalated in the copolymer chains were able to transfer and store energy well, but GO sheets that were too rigid stacked the links of the polymer and hindered the movement of the segments.

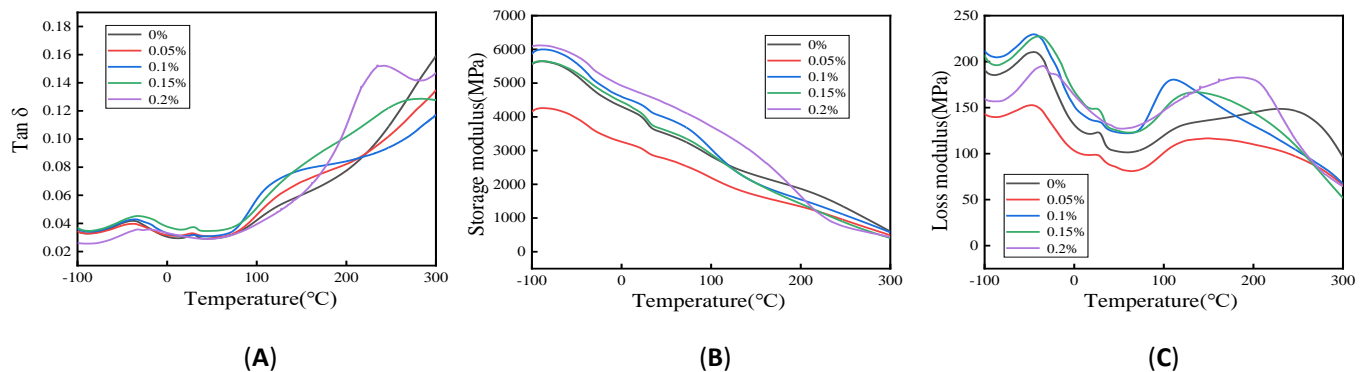


Figure 4. $\text{Tan}\delta$ (A), storage modulus (B), and loss modulus (C)—temperature curves of GO hybrid PU–PF copolymers with different GO content.

In Figure 4A, the difference in $\text{Tan}\delta$ is very small at room temperature, but was significantly enlarged in the 100–150 °C zone. The maximum belonged to the sample of 0.1 wt% GO content, and the $\text{Tan}\delta$ values of samples of 0.15 wt%, 0.05 wt%, 0 wt%, and 0.2 wt% decreased sequentially. In fact, at this temperature range, the copolymers began to soften and partial areas to melt, so some segments and molecules obtained enough energy to move. Figure 4C indicates that the loss modulus of the 0.1 wt% GO-content sample increased more significantly than other samples in 100–150 °C range, due to the homogeneous dispersion of the GO pieces between the molecular chains creating a strong intermolecular force that hindered the thermal movement of the molecular chains. By comparison, we found the change trend in $\text{Tan}\delta$ of different GO content in the range of 100–150 °C was similar to that of DSC and mechanical properties. The experimental results were mutually confirmed.

3.3. Tribological Character

Dry sliding behavior of PU, PF, and PU–PF with 10 wt% PU content and the GO (0.1 wt%) hybrid PU (10 wt%)–PF copolymer during friction are displayed in Figure 5. It can be seen that the PU curve exhibits great noise, The curve of the PU–PF copolymer is very smooth, and the curves of PF and GO hybrid PU–PF copolymers are a little rough. Average friction coefficients (COFs) were calculated and are listed in Table 3. The COF of the PU–PF copolymer was 0.58, which lay in an intermediate position between pure PF (0.3) and PU (1.03). With the aim of understanding the tribology mechanism, the worn surfaces of sliding friction samples of PU, PF, PU–PF, and GO hybrid PU–PF copolymers were detected by SEM, as shown in Figure 6. Figure 6a shows the morphology of the worn surface of pure PU. It can be seen that the PU surface was damaged homogeneously. Only some slim ridges were left when the counterpart was moved away. Signs of melting can be seen on the edges of ridges. Evidently, the most of material on the surface has been worn off and melt under frictional heat. The friction mechanism of PU was classified as adhesion wear, since the surface was mainly damaged by viscous tearing. The friction force was very unstable during the friction process, which could explain the great noise in the PU sliding curve, while there were lots of fish scale-like protrusions on the worn surface of

pure PF in Figure 6b, with slight peeling of the epidermis. Owing to outstanding thermal stability, stiffness, and mechanical strength, the surface of PF resin was not easily destroyed. Only on some microscopic protrusions was frictional resistance increased, leading to some surface layers being scraped off. The fluctuation in frictional resistance was deemed to be the reason that the sliding curve of PF in Figure 5 was relatively rough. Above all, the friction mechanism of PU belongs to abrasive and fatigue wear mechanisms. On the worn surface of the PU–PF copolymer in Figure 6c, more severe surface detachment has occurred, and some relatively deep furrow traces appear in the detachment area. This phenomenon was caused by the soft–hard phase-combination structure of PU–PF on the surface, where the PF phase formed the hard region and the PU phase formed the soft region. When the surface was exposed to the counterpart pressure, the PU soft region was depressed via elastic deformation, while the PF hard region could not deform, so the hard region was ploughed into the soft region by the counterpart pin. The situation was changed by the addition of GO. As displayed in Figure 6d, the worn surface of the GO hybrid PU–PF copolymer appeared relatively intact, with only some shallow scratches appearing. Upon investigation, we believed that since the hybrid of GO enhanced the hardness and strength of the whole PU–PF copolymer, the PU soft region was also reinforced, so its surface resistance to friction damage was stronger. There were also lots of fish scale-like protrusions on it, which induced uneven frictional resistance resulting in a relatively rough sliding curve of the GO hybrid PU–PF copolymer in Figure 5.

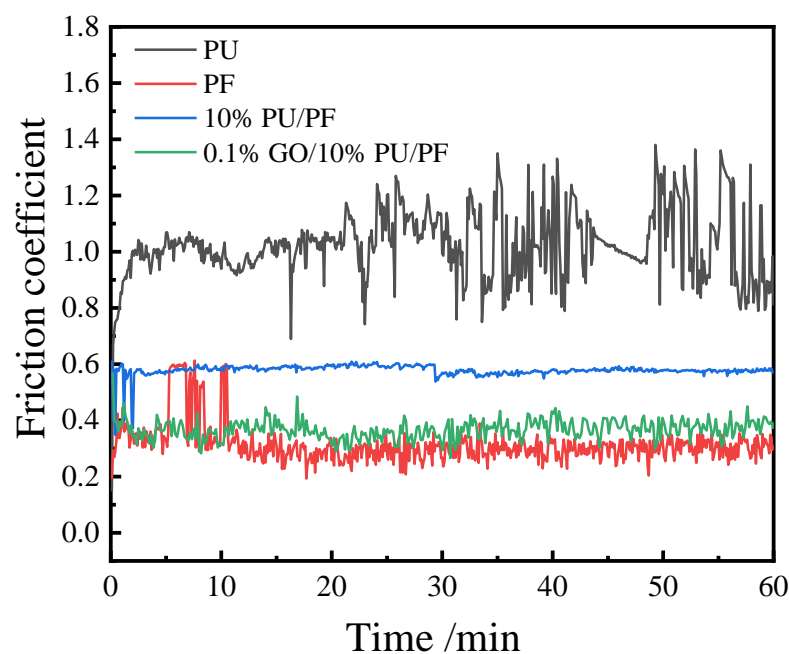


Figure 5. Sliding behavior curves of PU, PF, and PU–PF copolymers during wearing process.

Table 3. COFs of PU, PF, and PU–PF and GO hybrid PU–PF copolymers.

Resin Type	PU	PF	10%PU–PF	0.05%GO + 10%PU–PF	0.1%GO + 10%PU–PF	0.15%GO + 10%PU–PF	0.2%GO + 10%PU–PF
COFs	1.03	0.3	0.58	0.42	0.37	0.4	0.39

The dry sliding behavior of GO hybrid PU–PF copolymers with different GO content is illustrated in Figure 7, with the COF curve in the inset. This indicates that COFs of the copolymers were reduced by GO hybridization. When GO addition was 0.1 wt%, the COF was at its minimum of 0.37. The specific wear rate (listed in Table 4) revealed the same tendency with COFs. Likewise, the 0.1 wt% GO-content sample showed the lowest value

($1.16 \times 10^{-4} \text{ mm}^3/\text{Nm}$), which was reduced by 73.5% compared with that of the PU–PF copolymer without GO hybrid ($4.38 \times 10^{-4} \text{ mm}^3/\text{Nm}$).

Table 4. Specific wear rate of PU, PF, and PU–PF and GO hybrid PU–PF copolymers.

Resin Type	PU	PF	10%PU–PF	0.05%GO + 10%PU–PF	0.1%GO + 10%PU–PF	0.15%GO + 10%PU–PF	0.2%GO + 10%PU–PF
Specific wear rate ($10^{-4} \text{ mm}^3/\text{Nm}$)	53.44	3.13	4.38	2.77	1.16	1.7	1.89

An interesting phenomenon can be observed in Figure 7 where all the sliding curves of GO hybrid PU–PF copolymers converge together independently of GO content, indicating almost the same COF. This result was consistent with our previous research, and the reasons for this are analyzed in detail in our previous published papers [44,45]. The most important observation was that the identical steady friction coefficients of GO hybrid PU–PF copolymers with different GO contents were derived from the same friction bodies in the three-body friction model, which were composed of the GO-strengthened PU–PF copolymer surface, the metallic counterpart, and the GO-wrapping polymer particles as the wear debris in the transfer film.

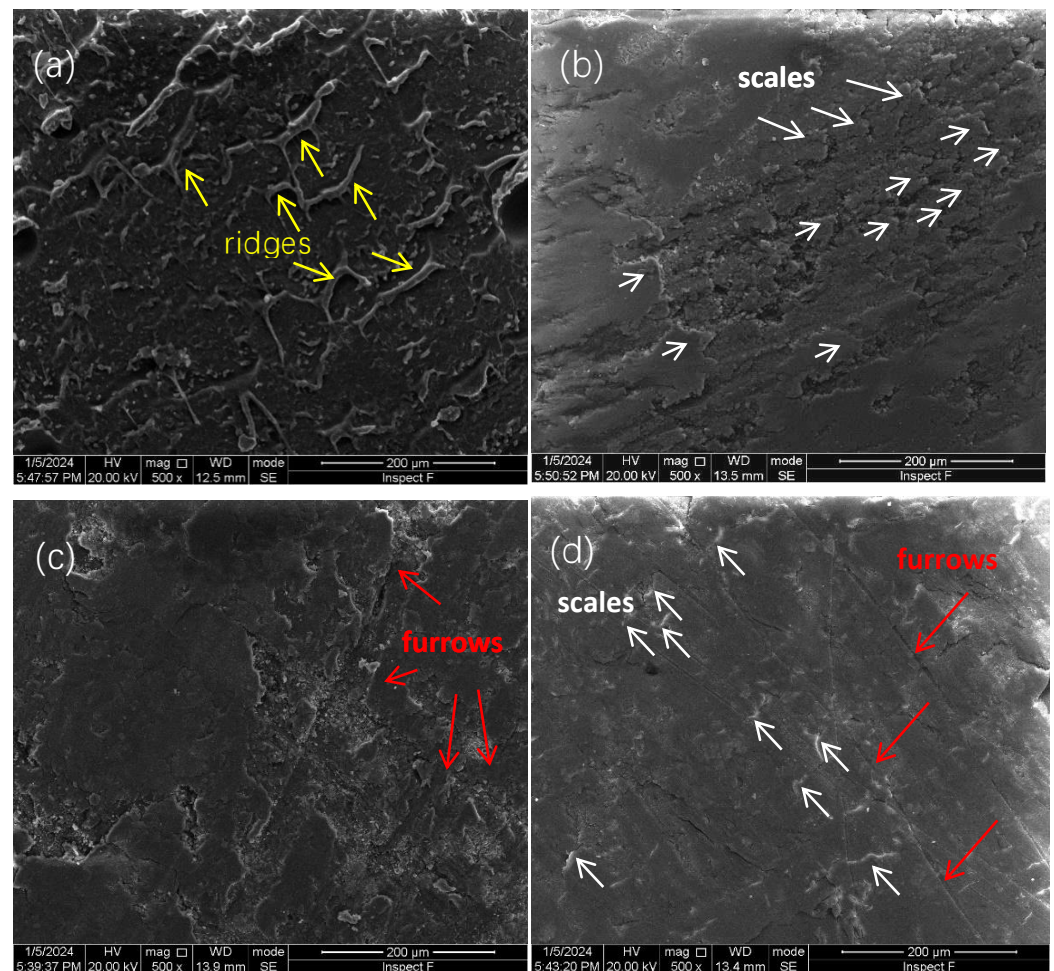


Figure 6. SEM pictures of worn surfaces of PU (a), PF (b), and PU–PF (c) and GO hybrid PU–PF copolymers (d). (yellow arrows for ridges, white arrows for scales, red arrows for furrows).

To verify the observations above, the substance distribution on the worn surface of the PU–PF copolymers with and without GO hybrid samples was tested by Raman mapping,

as shown in Figure 8. Both tests were focused on the interface between friction and non-friction areas. The two images present two completely different phenomena. There is a uniform picture on the surface of PU–PF copolymers without GO hybrid in Figure 8A, with no difference between the friction surface and non-friction surface. A small number of PU components (blue dots) are evenly distributed in the PF matrix (red area). However, it is completely different on the surface of PU–PF copolymers with GO hybrid in Figure 8B: the components on the friction and non-friction surfaces are clearly different. The friction area shows a large amount of GO component coverage. This result was consistent with our previous research findings on GO hybrid PU–EP IPNs [44]. In the GO hybrid complex, the GO components gathered on the friction surface to form a GO transfer film after a period of friction, which meant the friction behavior changed from dry friction to boundary friction. That could be another explanation for why the COFs of composites with different GO content were very close.

By comparing the frictional performance of the GO hybrid PU–PF materials with those of materials (GO hybrid PU–EP) in the literature [44,45], similar results were obtained, which has beneficial theoretical value for the promotion and application of GO hybrid composite materials in the field of friction and wear. Due to its superior strength and heat resistance, the GO hybrid PU–PF material was more suitable for precision grinding of difficult-to-machine metal materials such as bearing steel than the GO hybrid PU–EP materials, so in this study, we explored the precision machining property of GO hybrid PU–PF materials.

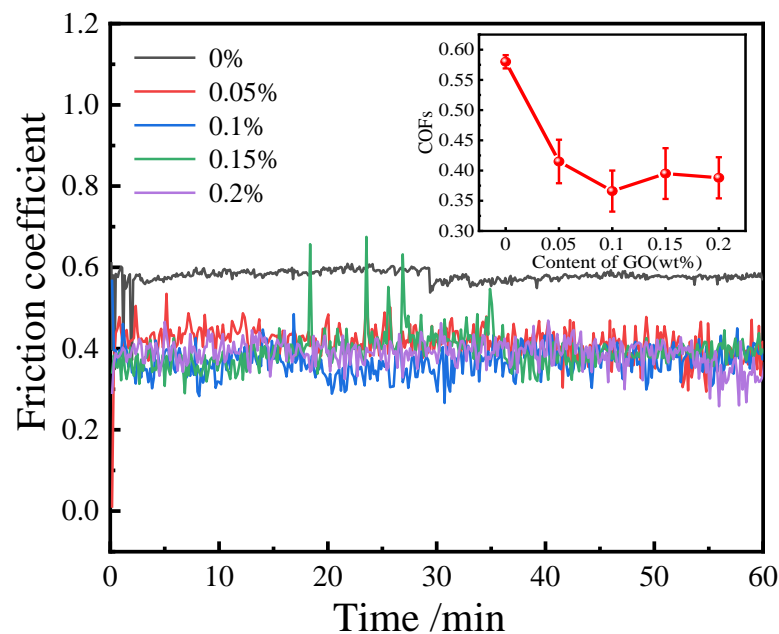


Figure 7. Sliding behavior curves (inset: COFs) of GO hybrid PU–PF copolymers with different GO content during wearing process.

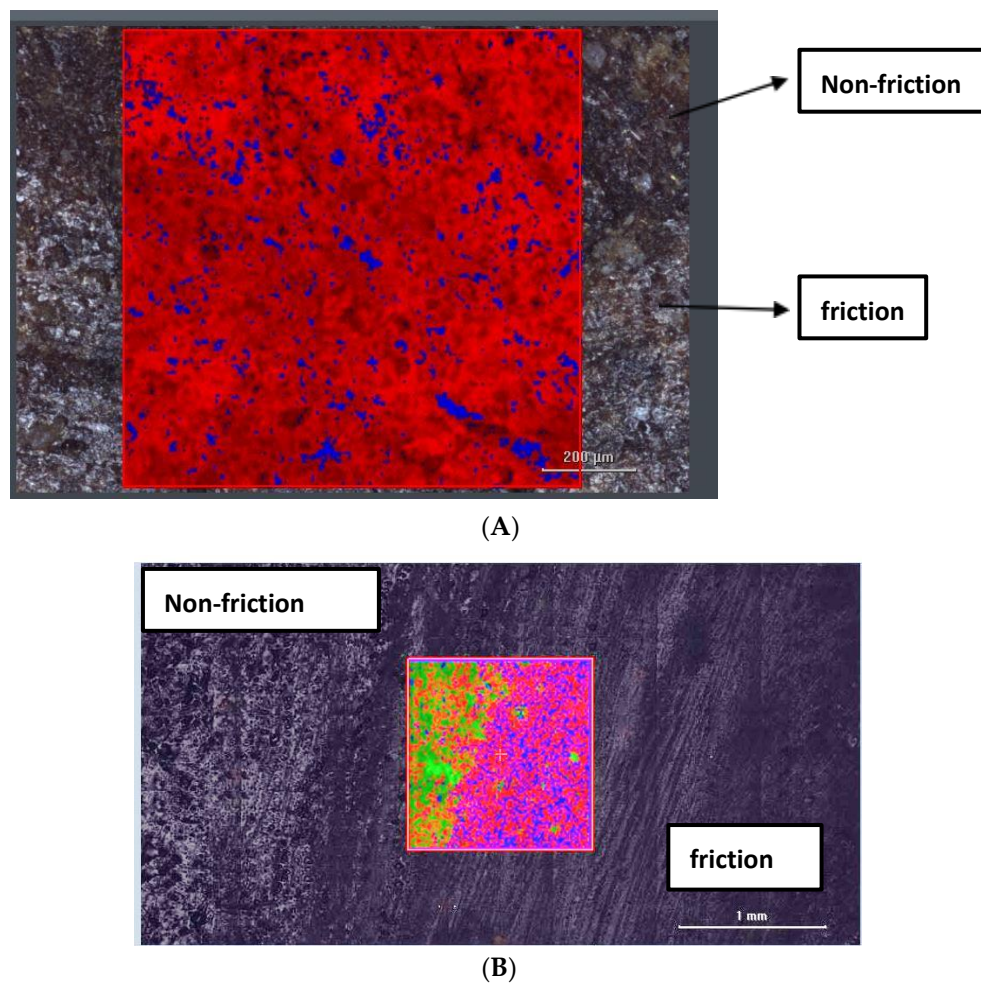
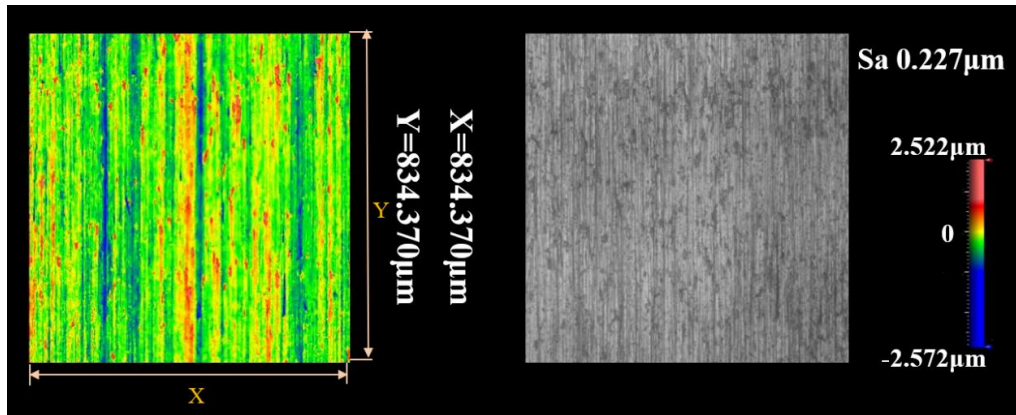


Figure 8. Raman mapping images of PU–PF copolymers without (A) and with (B) GO hybrid sample surfaces before and after friction.

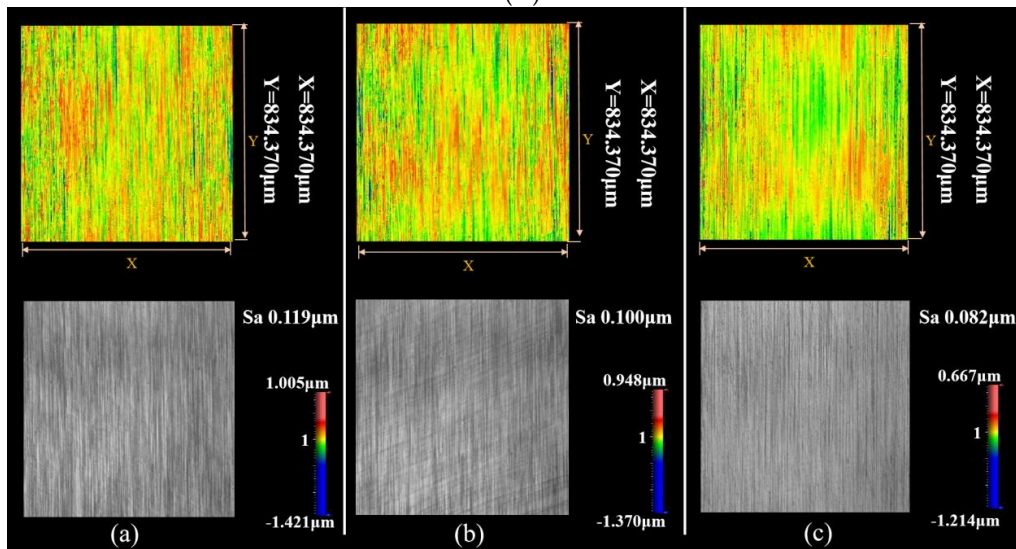
3.4. Precision Machining

Three types of grinding wheels were manufactured using pure PU, PU–PF, and GO hybrid PU–PF as matrix material. Corundum was applied as abrasive, and for each matrix type, three corundum particle sizes of w14, w10, and w5 were selected to manufacture grinding wheels, respectively. Therefore, a total of nine grinding wheel samples were prepared and machining tests were conducted on high-carbon chromium bearing steel GCr15 workpieces. The surface roughness (Ra) of the workpieces before and after machining was measured using white-light interferometry, as shown in Figure 9. The resultant values of surface roughness (Ra) are shown in Figure 10A. It was found that no matter which particle-size grinding wheel was used for machining, the Ra of the workpiece was significantly reduced. The finer the particle size of corundum abrasive, the lower the surface roughness of the workpiece. For grinding wheels of the same particle size, GO hybrid PU–PF grinding wheels had the lowest Ra, followed by PU-modified PF. This was consistent with our prediction. PU modification improved the damping and vibration reduction performance of the grinding wheel matrix material PF. During the machining process, the friction force between the grinding wheel and the workpiece was more uniform and stable, resulting in uniform removal of micro-roughness on the workpiece surface, resulting in lower surface roughness of the workpiece. The hybridization of GO further improved the damping characteristics of the grinding wheel substrate material, and formed a transfer film between the tool and the workpiece during the machining process, which further reduced the grinding force and was more conducive to obtaining high-quality surfaces.

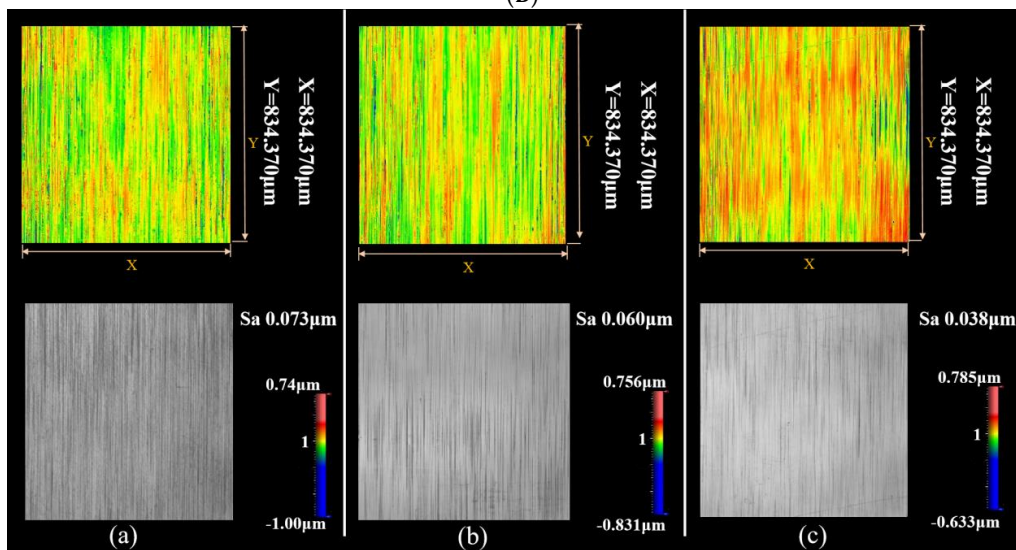
After grinding with the GO hybrid PU–PF grinding wheel with a corundum particle size of w5, the Ra value of the high-carbon chromium bearing steel GCr15 workpiece was reduced to 29 nm, which was 35% lower than that of pure PF grinding wheels.



(A)



(B)



(C)

Figure 9. Cont.

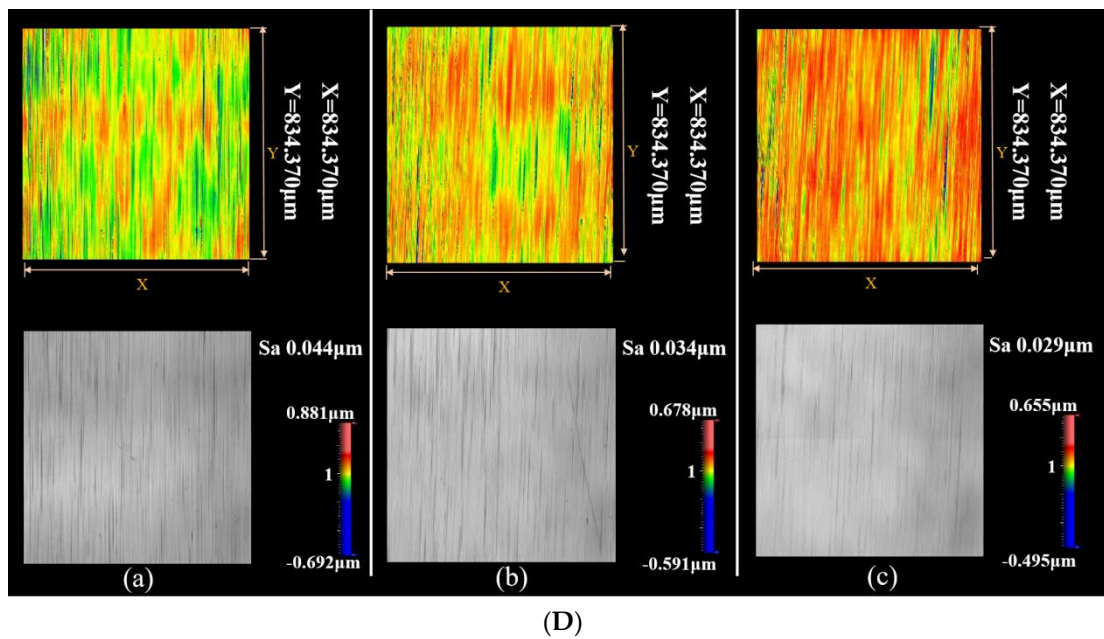


Figure 9. White-light interference pattern on the surface of workpieces before (A) and after machining by grinding wheels made of pure PF (a), PU–PF (b), and GO hybrid PU–PF (c) with corundum particle sizes of w14 (B), w10 (C), and w5 (D).

In Figure 10B, the grinding sharpness of grinding wheels made of pure PF, PU–PF and GO hybrid PU–PF copolymers with different corundum particle sizes (w14, w10, and w5) are also evaluated. During the machining process, the reduction in diameter of axial workpieces per unit time was used to measure the sharpness of the grinding wheel. The results showed that the sharpness of both grinding wheels made of PU–PF and GO hybrid PU–PF were much higher than that of pure PF, and the sharpness of the grinding wheel made of PU–PF was the maximum.

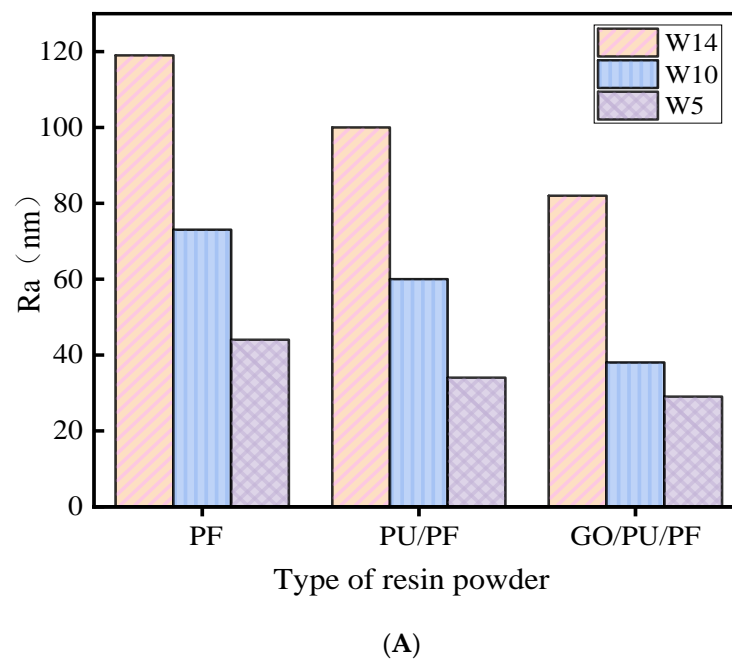
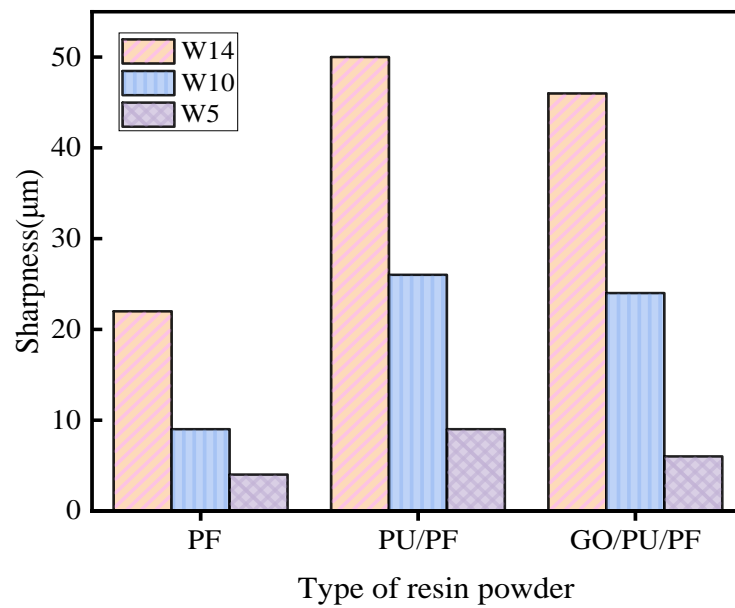


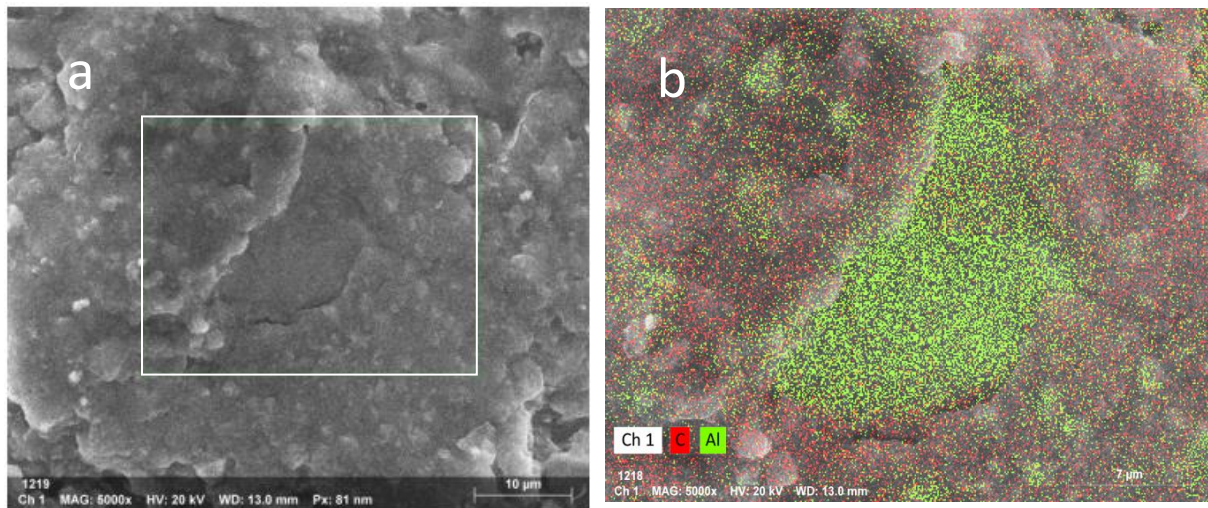
Figure 10. Cont.



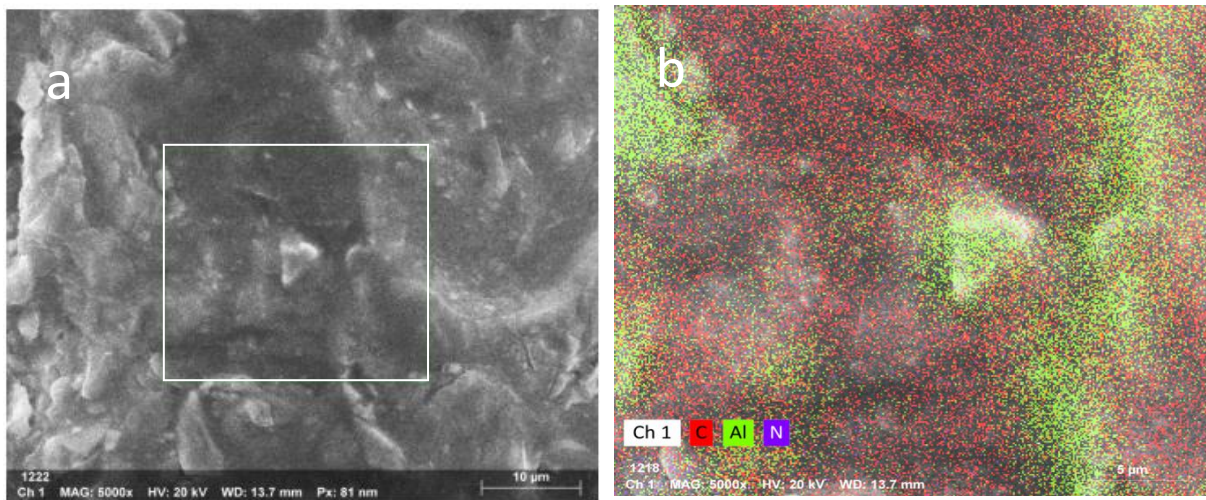
(B)

Figure 10. Surface roughness (Ra) of workpieces (A) and grinding sharpness (B) machined by grinding wheels made of pure PF, PU–PF, and GO hybrid PU–PF copolymers with different corundum particle sizes (w14, w10, and w5).

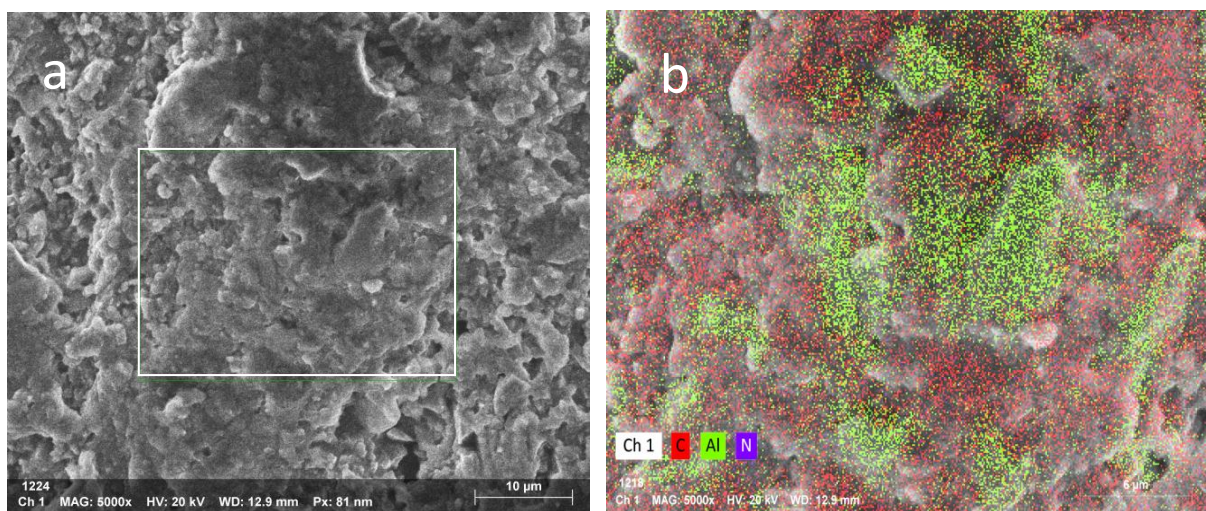
In order to explore the mechanism for improving the machining effect, SEM and EDS mapping was conducted on the grinding surface of the grinding wheel with corundum particle sizes of w14, as shown in Figure 11. By comparing with the images on the left, it can be observed that there are significant differences in the grinding surfaces of the three types of grinding wheels. For the grinding wheel made of pure PF, the grinding surfaces look relatively flat and smooth. The grinding wheel of PU–PF appears somewhat uneven, with many protrusions of corundum particles on the surface looking like mountain ridges. For that of GO hybrid PU–PF, it became rougher with many micro-gaps, and the EDS mapping graph (Figure 11(Cb)) shows that the corundum abrasive was more evenly wrapped by the resin. The formation cause could be very complex. It may be related to the viscosity and interactions between components. We will carry out further research specifically on this issue. However, the morphology described above could well explain the difference in sharpness of the grinding wheels. The mountain ridges formed by corundum particle edges just like blades cut the workpiece sharply, allowing the substance on the surface of the workpiece to be quickly ground off. As for the slightly lower sharpness of GO hybrid PU–PF grinding wheels compared to that of PU–PF, the reason was speculated to be that the lubricating effect of GO reduced the grinding force to a certain extent, which resulted in the reduction in sharpness.



(A)



(B)



(C)

Figure 11. EDS pictures of grinding wheels made of pure PF (A), PU-PF (B), and GO hybrid PU-PF (C). (graph b is the energy mapping of the white box area in graph a).

Figure 12 displays Al and N element distribution maps of grinding wheels made of PU–PF and GO hybrid PU–PF. The N element came from –NCO groups in PU chains, and Al from the corundum abrasive (Al_2O_3). For the N element distribution maps in Figure 12(Ab,Bb), one can see upon careful observation that both images show that the N atoms are not uniformly dispersed outside the corundum region, but arranged in a linear pattern. Also, the contour profile matches the edge position of the corundum abrasive to a large extent. After analysis, we speculated that this was caused by the strong intermolecular forces generated from carbonyl and amino groups in the PU molecular chain and the Al–O bond on the surface of the corundum abrasive, since all of them possess strong polarity. As such, the PU component tended to be dispersed around the edges of the corundum abrasive, acting as a buffer layer of abrasive particles, as depicted in Figure 13. This distribution provided micro damping characteristics for the abrasive, which could play a role in buffering the grinding force on the abrasive, making the grinding force on the workpiece more stable during precision machining and thus achieving smoother surface quality of the workpiece. This discovery has great significance and provides a scientific basis for the design and fabrication of precision machining tools.

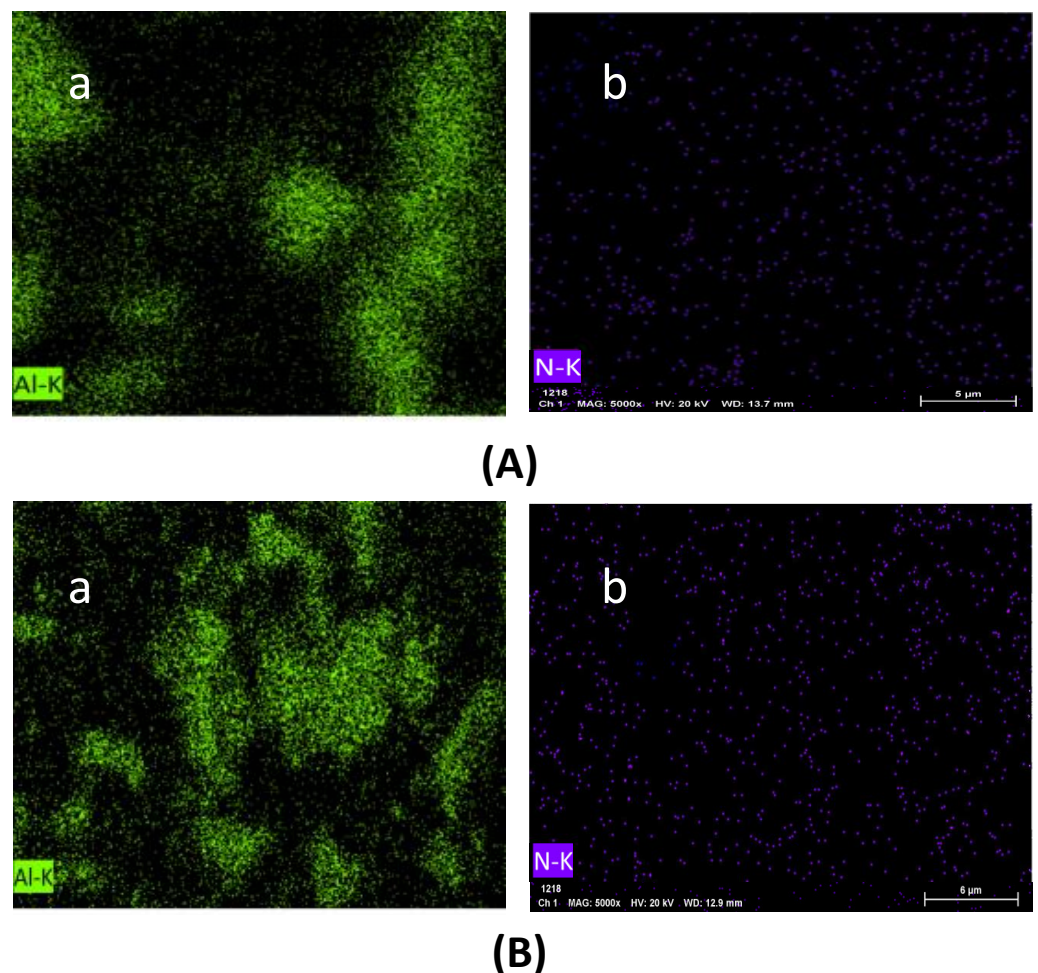


Figure 12. Al (a) and N (b) element distribution maps of grinding wheels made of PU–PF (A) and GO hybrid PU–PF (B).

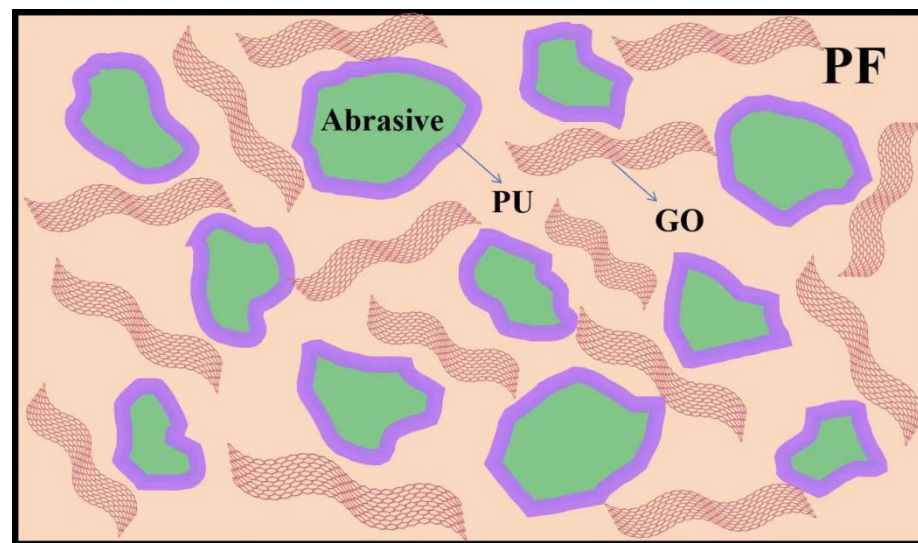


Figure 13. Component distribution diagram of grinding wheels made of GO hybrid PU–PF.

4. Conclusions

To understand the influence of damping and friction performance of grinding wheels on precision grinding, GO hybrid PU-modified PF copolymers were prepared by in situ synthesis. The optimal performance of the copolymer was achieved when the PU addition was 10 wt% and the GO addition was 0.1 wt%. With this ratio, the bending strength of 0.1% GO hybrid PU–PF was increased by 14.8% and the impact strength was increased by 18.8% compared to the PU–PF copolymer without GO hybrid. DMA results displayed small glass transition peaks on the curve of PU–PF and GO hybrid PU–PF copolymers, which meant the PU ingredients endowed the modified PF micro damping properties.

The sliding behavior of the GO hybrid PU–PF copolymers was displayed when GO addition was 0.1 wt% and the COF was at its minimum of 0.37. COFs of the copolymers with different GO content were very similar. Likewise, the 0.1 wt% GO-content sample obtained the lowest value, $1.16 \times 10^{-4} \text{ mm}^3/\text{Nm}$, which was 73.5% less than that of the PU–PF copolymer without GO hybrid ($4.38 \times 10^{-4} \text{ mm}^3/\text{Nm}$).

Grinding wheels were manufactured using pure PU, PU–PF, and GO hybrid PU–PF as matrix material. Machining tests were conducted on high-carbon chromium bearing steel GCr15 workpieces. GO hybrid PU–PF grinding wheels significantly reduced the surface roughness of the workpiece. The sharpness of both grinding wheels made of PU–PF and GO hybrid PU–PF was much higher than that of pure PF. Raman mapping images provided favorable evidence for the formation of GO transfer film during the friction process. EDS mapping revealed the PU component tended to be dispersed around the edges of the corundum abrasive, acting as a buffer layer of abrasive particles. It was supposed to provide micro damping characteristics for abrasives, making the grinding force more stable during precision machining and facilitating smoother surface quality of the workpiece. This discovery provides a scientific basis for the design and preparation of precision grinding tools.

Author Contributions: Conceptualization, S.X.; Methodology, Y.L.; Software, S.G.; Validation, Y.J. and J.L.; Formal analysis, X.S.; Investigation, H.Z.; Data curation, J.P.; Writing—review & editing, C.L.; Funding acquisition, J.X. All authors have read and agreed to the published version of the manuscript.

Funding: This research was funded by Henan Province Science and Technology Research Projects (242102230179), Henan Province Undergraduate Innovation and Entrepreneurship Training Program Project (221071000210), the Key R & D projects of Henan Province (241111233100) and Langfang Shengsen Grinding Tools Co., Ltd.

Institutional Review Board Statement: Not applicable.

Informed Consent Statement: Not applicable.

Data Availability Statement: Data are contained within the article.

Conflicts of Interest: Author Jixian Xu was employed by the company Langfang Shengsen Grinding Tools Co., Ltd. The remaining authors declare that the research was conducted in the absence of any commercial or financial relationships that could be construed as a potential conflict of interest.

References

1. Brinksmeier, E.; Mutlugünes, Y.; Ohmori, H. Ultra-precision grinding. *CIRP Ann.* **2010**, *59*, 652–671. [\[CrossRef\]](#)
2. Lee, E.S.; Baek, S.Y. A study on optimum grinding factors for aspheric convex surface micro-lens using design of experiments. *Int. J. Mach. Tool. Manuf.* **2007**, *47*, 509–520. [\[CrossRef\]](#)
3. Yan, Y.; Zhang, Z.; Liu, J. Study on the algorithm of three-dimensional surface residual material height of nano-ZrO₂ ceramics under ultra-precision grinding. *Micromachines* **2021**, *12*, 1363. [\[CrossRef\]](#) [\[PubMed\]](#)
4. Xu, J.; He, Q.; Zhang, X. Euler's equation grinding track. microgrinding mechanism, and process research of space optical crystal materials. *Int. J. Adv. Manuf. Technol.* **2023**, *128*, 5209–5221. [\[CrossRef\]](#)
5. Jahnel, K.; Michels, R.; Wilhelm, D.P. Investigation of surface integrity induced by ultra-precision grinding and scratching of glassy carbon. *Micromachines* **2023**, *14*, 2240. [\[CrossRef\]](#)
6. Wang, S.; Zhao, Q.; Wu, T. An investigation of monitoring the damage mechanism in ultra-precision grinding of monocrystalline silicon based on AE signals processing. *J. Manuf. Process.* **2022**, *81*, 945–961. [\[CrossRef\]](#)
7. Kakinuma, Y.; Konuma, Y.; Fukuta, M. Ultra-precision grinding of optical glass lenses with La-doped CeO₂ slurry. *CIRP Ann.* **2019**, *68*, 345–348. [\[CrossRef\]](#)
8. Jiang, C.; Li, H.; Mai, Y. Material removal monitoring in precision cylindrical plunge grinding using acoustic emission signal. *Proc. Inst. Mech. Eng. Part C J. Mech. Eng. Sci.* **2014**, *228*, 715–722. [\[CrossRef\]](#)
9. Sun, Z.; Guan, C.; Dai, Y. Ultra-precision time-controlled grinding for flat mechanical parts with weak stiffness. *J. Manuf. Process.* **2023**, *99*, 105–120. [\[CrossRef\]](#)
10. Monier, A.; Guo, B.; Zhao, Q. Effects of the grinding conditions on geometry of microstructured surfaces fabricated via designed precision grinding. *Proc. Inst. Mech. Eng. Part B J. Eng. Manuf.* **2023**, *237*, 573–587. [\[CrossRef\]](#)
11. Xiao, G.; Huang, Y. Adaptive belt precision grinding for the weak rigidity deformation of blisk leading and trailing edge. *Adv. Mech. Eng.* **2017**, *9*, 1687814017731705. [\[CrossRef\]](#)
12. Cai, R.; Wan, N.; Mo, R. Prediction of un-uniform grinding wheel wear based on instantaneous engagement of multi-axis grinding. *Int. J. Adv. Manuf. Technol.* **2022**, *119*, 3407–3425. [\[CrossRef\]](#)
13. Brecher, C.; Baumler, S.; Brockmann, B. Avoiding chatter by means of active damping systems for machine tools. *J. Mach. Eng.* **2013**, *13*, 117–128.
14. Bianchi, G.; Cagna, S.; Cau, N. Analysis of vibration damping in machine tools. *Procedia CIRP* **2014**, *21*, 367–372. [\[CrossRef\]](#)
15. Ghorbani, S.; Polushin, N.I. Effect of composite material on damping capacity improvement of cutting tool in machining operation using taguchi approach. *Eng. Technol. Int.* **2015**, *9*, 1339–1349.
16. Devin, L.N.; Osadchii, A.A. Improving performance of CBN cutting tools by increasing their damping properties. *J. Superhard Mater.* **2012**, *34*, 328–335. [\[CrossRef\]](#)
17. Sexton, J.S.; Howes, T.D.; Stone, B.J. The use of increased wheel flexibility to improve chatter performance in grinding. *Proc. Inst. Mech. Eng.* **1982**, *196*, 291–300. [\[CrossRef\]](#)
18. Shen, R.; Qian, X.; Zhou, J. Characteristics of passive vibration control for exponential non-viscous damping system: Vibration isolator and absorber. *J. Vib. Control.* **2023**, *29*, 5078–5089. [\[CrossRef\]](#)
19. Zhu, L.; Hao, J.; Lu, L. Research on influence of damping on the vibration noise of transformer. *IEEE Access* **2022**, *10*, 92128–92136. [\[CrossRef\]](#)
20. Shum, K.M. Tuned vibration absorbers with nonlinear viscous damping for damped structures under random load. *J. Sound. Vib.* **2015**, *346*, 70–80. [\[CrossRef\]](#)
21. Chen, S.; Yang, Z.; Ying, M. Parallel load-bearing and damping system design and test for satellite vibration suppression. *Appl. Sci.* **2020**, *10*, 1548. [\[CrossRef\]](#)
22. Luo, H.; Guo, S.; Yu, C. Vibration suppression analysis and experimental test of additional constrained damping layer in space science experiment cabinet. *Compos. Adv. Mater.* **2021**, *30*, 2633366X20978659. [\[CrossRef\]](#)
23. Gou, Z.; Li, B.; Fei, J. Frictional characteristics and vibration behavior of silicone rubber powders modified resin-based friction materials. *J. Appl. Polym. Sci.* **2024**, *141*, e55344. [\[CrossRef\]](#)
24. Babkina, N.; Antonenko, O.; Kosyanchuk, L. Effect of polyurethane material design on damping ability. *Polym. Adv. Technol.* **2023**, *34*, 3426–3437. [\[CrossRef\]](#)
25. Sain, T.; Yeom, B.; Waas, A.M. Effect of soft segment and clay volume fraction on rate dependent damping of polyurethane and polyurethane-clay nanocomposites. *J. Reinf. Plast. Comp.* **2014**, *33*, 2129–2135. [\[CrossRef\]](#)

26. Khanouki, M.A.; Ohadi, A. Improved acoustic damping in polyurethane foams by the inclusion of silicon dioxide nanoparticles. *Adv. Polym. Technol.* **2018**, *37*, 2799–2810. [CrossRef]
27. Li, L.; Tian, B.; Li, L. Preparation and characterization of silicone oil modified polyurethane damping materials. *J. Appl. Polym. Sci.* **2019**, *136*, 47579. [CrossRef]
28. Chen, S.; Wang, Q.; Wang, T. Preparation, tensile, damping and thermal properties of polyurethanes based on various structural polymer polyols: Effects of composition and isocyanate index. *Polym. Res.* **2012**, *19*, 9994. [CrossRef]
29. Shi, M.; Zheng, J.; Huang, Z. Synthesis of polyurethane prepolymers and damping property of polyurethane/epoxy composites. *Adv. Sci. Lett.* **2014**, *4*, 740–744. [CrossRef]
30. Su, Y.; Li, T.; Liu, Y. Mechanical and damping properties of graphene-modified polyurethane-epoxy composites for structures. *Polym-Korea* **2021**, *45*, 483–490. Available online: <https://10.7317/pk.2022.45.4.483> (accessed on 26 July 2021). [CrossRef]
31. Zhang, C.; Chen, Y.; Li, H. Facile fabrication of polyurethane/epoxy IPNs filled graphene aerogel with improved damping, thermal and mechanical properties. *RSC Adv.* **2018**, *8*, 27390–27399. [CrossRef]
32. Feng, Q.; Shen, M.; Zhu, J. Realization of polyurethane/epoxy interpenetrating polymer networks with a broad high-damping temperature range using β -cyclodextrins as chain extenders. *Mater. Des.* **2021**, *212*, 110208. [CrossRef]
33. Yu, W.; Zhang, D.; Du, M. Role of graded length side chains up to 18 carbons in length on the damping behavior of polyurethane/epoxy interpenetrating polymer networks. *Eur. Polym. J.* **2013**, *49*, 1731–1741. [CrossRef]
34. Chen, S.; Wang, Q.; Pei, X. Dynamic mechanical properties of castor oil-based polyurethane/epoxy graft interpenetrating polymer network composites. *J. Appl. Polym. Sci.* **2010**, *118*, 1144–1151. [CrossRef]
35. Chen, S.; Wang, T.; Wang, Q. Studies on tribological, damping and thermal properties of polyurethane/polystyrene interpenetrating polymer networks. *J. Polym. Mater.* **2016**, *33*, 503–512.
36. Wang, Q.; Chen, S.; Wang, T. Damping, thermal, and mechanical properties of polyurethane based on poly(tetramethylene glycol)/epoxy interpenetrating polymer networks: Effects of composition and isocyanate index. *Appl. Phys. A-Mater.* **2011**, *104*, 375–382. [CrossRef]
37. Qin, C.; Jin, Z.; Bai, X. Compatibility of polyurethane/(vinyl ester resin)(ethyl acrylate) interpenetrating polymer network. *Polym. J.* **2007**, 1365–1372. [CrossRef]
38. Statharas, E.C.; Yao, K.; Rahimabady, M. Polyurethane/poly(vinylidene fluoride)/MWCNT composite foam for broadband airborne sound absorption. *J. Appl. Polym. Sci.* **2019**, *136*, 47868. [CrossRef]
39. Xu, X.; Huang, S.; Guan, J. Grinding performance and self-lubrication mechanism of phenolic resin-bonded grinding wheel filled with inclusion complex of β -cyclodextrin and dialkyl pentasulfide. *J. Mater. Process Technol.* **2015**, *221*, 163–171. [CrossRef]
40. Bashandeh, K.; Lan, P.; Meyer, J.L. Tribological performance of graphene and PTFE solid lubricants for polymer coatings at elevated temperatures. *Tribol. Lett.* **2019**, *67*, 99. [CrossRef]
41. Aliyu, I.K.; Mohammed, A.S.; Al-Qutub, A. Tribological performance of ultra high molecular weight polyethylene nanocomposites reinforced with graphene nanoplatelets. *Polym. Compos.* **2019**, *40*, E1301–E1311. [CrossRef]
42. Aliyu, I.K.; Mohammed, A.S.; Al-Qutub, A. Tribological performance of UHMWPE/GNPs nanocomposite coatings for solid lubrication in bearing applications. *Tribol. Lett.* **2018**, *66*, 144. [CrossRef]
43. Ma, C.; Shan, Y.; Wang, N. High-damping polyurethane-based composites modified with amino-functionalized graphene. *High. Perform. Polym.* **2023**, *35*, 795–811. [CrossRef]
44. Xia, S.; Liu, Y.; Pei, F. Identical steady tribological performance of graphene-oxide-strengthened polyurethane/epoxy interpenetrating polymer networks derived from graphene nanosheet. *Polymer* **2015**, *64*, 62–68. [CrossRef]
45. Yue, R.; Liu, Y.; Xia, S. Raman imaging evidence for mechanical/tribological quasi-steady state in GO strengthening polyurethane/epoxy interpenetrating polymer network. *Macromol. Res.* **2022**, *30*, 477–485. [CrossRef]
46. Zhang, H.Y.; Xia, S.L.; Liu, C. In-situ closed synthesis of phenolic resin from PPU and its damping properties. *Comp. Sci. Eng.* **2024**, 1–9. Available online: <http://kns.cnki.net/kcms/detail/10.1683.TU.20240227.1807.006.html> (accessed on 23 November 2023). [CrossRef]
47. GB/T 528-1998; Rubber, Vulcanized or Thermoplastic—Determination of Tensile Stress-Strain Properties [Including MODIFICATION 1]. Ministry of Chemical Industry of the People Republic of China: Beijing, China, 1998.

Disclaimer/Publisher’s Note: The statements, opinions and data contained in all publications are solely those of the individual author(s) and contributor(s) and not of MDPI and/or the editor(s). MDPI and/or the editor(s) disclaim responsibility for any injury to people or property resulting from any ideas, methods, instructions or products referred to in the content.